D004

Computation of Elastic Properties Based on Microtomogram Images

V. Shulakova* (CSIRO), M. Pervukhina (CSIRO), M. Lebedev (Curtin University), T. Mueller (CSIRO), S. Mayo (CSIRO), S. Schmid (CSIRO), B. Clennell (CSIRO) & B. Gurevich (Curtin University)

SUMMARY

Understanding of physical rock properties is currently of great importance both for industry and fundamental science, for it allows improving interpretation and reducing risks. Digital rock physics provides us with a promising opportunity for rock analysis and quantification. Moreover it allows running simulations on rock samples unsuitable for laboratory experiments. A detailed computational rock physics workflow including 3D rock imaging, processing and simulations of physical experiments has been created and tested on different rock samples. Here we describe this workflow and demonstrate the results of elastic simulation in comparison with experimental data obtained in physical laboratory for a sandstone sample.

Introduction

Finding relationship between rock microstructure and elastic properties is important or a better understanding and interpretation of seismic and well-logging data. Porous rocks have a very complex structure which comprises rock matrix, type of pore fluids, pore and grain shapes, grain contacts, pore connectivity. All of these factors affect the elastic response. Thus it is of great importance to have an accurate quantitative description of a complex microstructure of porous rocks.

Roberts and Garboczi (2000) suggested solving the equations of elasticity using finite element modeling (FEM) directly for microstructure obtained from computer tomography (CT). Based on the FEM algorithm developed by Garboczi (1998), Arns et al. (2002) derived elastic moduli - porosity relationships from microtomograms of Fontainebleau sandstone. A similar approach is adopted by Ingrain Inc. (e.g., Dvorkin, 2009). To simulate elastic wave propagation in digital rock, Saenger (2007) employed the finite-difference method with a rotated staggered grid. Each of these algorithms was specifically designed to simulate the elastic behaviour of highly heterogenerous structures consisting of a number of components with strongly contrasting processing.

In this work we propose a rock physics workflow including 3D imaging, processing and simulations of physical experiments that can be fulfilled using general-purpose and widely available software packages, namely, AVIZO (Visualization Sciences Group) and ABAQUS FEA (SIMULIA). Microtomograms obtained by a micro-CT scanner are first processed with AVIZO software including filtering, smoothing and segmentation into different phases. The obtained segmented tomograms are meshed and the resultant orphan mesh is saved in an ABAQUS input format. The meshed microstructure is imported into ABAQUS finite element analysis (FEA) software in which elastic moduli of a rock sample are numerically simulated. Finally, we compare the simulated moduli with the experimentally measured ones.

Data

A sample of well-consolidated felspathic Donnybrook sandstone with average porosity of 15% is used for studying elastic properties from micro-CT images. Three main constituents of the sample known from petrographic description are quartz, plagioclase feldspar and dissolved K-feldspar transformed to kaolinite. Volumetric fractions of quarts, plagioclase feldspar and kaolinite are determined from SEM images as 75%, 13% and 12%, respectively. The micro-CT images are obtained with the resolution of 2 μm. A cube of 400x400x400 pixels is cropped from the centre of the microtomogram and segmented into solid phase and pore space. Then the original cube is cropped into eight parts of 200^3 pixels each. Statistical analysis of these data shows that orientations of grains and pores in the sample are almost isotropic.

Image Processing

Throughout this paper we use 3D treatment of volume images as we noticed that 2D, slice-based processing can affect the geometry of the image features and cause undesired stripe-shape artefacts. First, to reduce noise level, we use edge preserve smoothing (AVIZO) which provides noise reduction without corruption of edges.

Cleaned volume is then subjected to segmentation routines that results in 3D digital representation of a number of phases existing in a particular rock sample. Segmentation is based on a simple threshold algorithm. The result of histogram-based segmentation into two phases (solid and pore space) for a fragment of Donnybrook sandstone is shown in Figure 1. In our case the solid phase consists of quartz, feldspar, and kaolinite. The mineral content is taken into account later during the simulation stage.

After assigning phase types ('grains' and 'pores' in our case), surfaces representing volume triangular approximation of phase interfaces is computed. As these surfaces contain a huge number of faces, they are then subjected to remeshing. The number of faces for each surface is reduced by factor 5 using the edge collapsing algorithm in AVIZO to the limit of approximately $2 \cdot 10^5$ faces and then remeshed using best isotropic algorithm with 50% faces reduction and constrained boundaries. This produces surfaces with approximately 10^5 faces.

a) 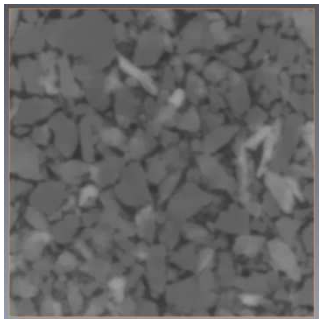 b) 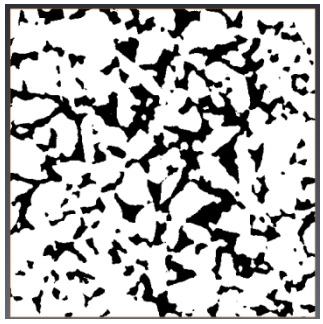

Figure 1: A tomographic slice of a 3D image of a sandstone sample: a) original greyscale image, b) its segmented image consists of two phases – matrix (white patterns) and pore space (black patterns).

Surface generation is followed by meshing of the volumes associated with the phases by generating volumetric tetrahedral grids. Each grid contains about $2 \cdot 10^6$ tetrahedral elements for each of the eight subvolumes of the original cube. Figure 2 shows meshing of one of the parts of Donnybrook sandstone; rock matrix and pore space are shown by blue and magenta colours, respectively.

a) 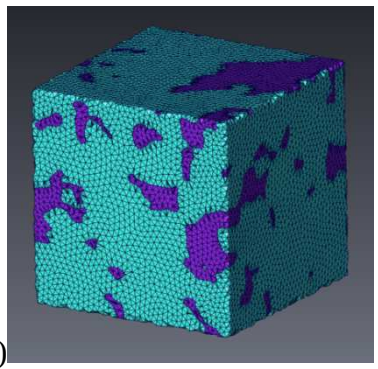 b) 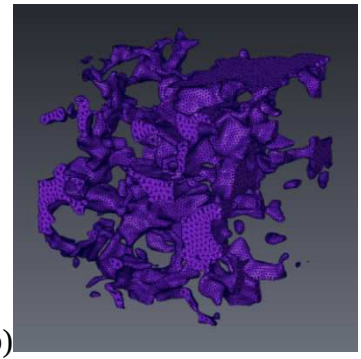 c) 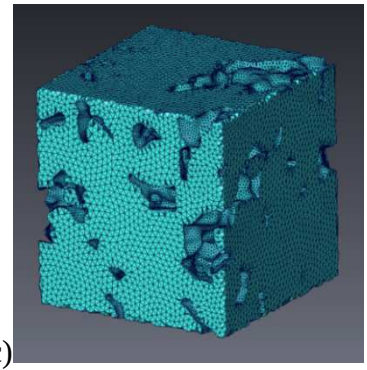

Figure 2: Volumetric tetrahedral mesh of one of eight 200^3 cubes of Donnybrook sandstone: (a) solid and pore phases, (b) pore space and (c) rock matrix.

Numerical simulation of effective bulk and shear moduli using microtomogram

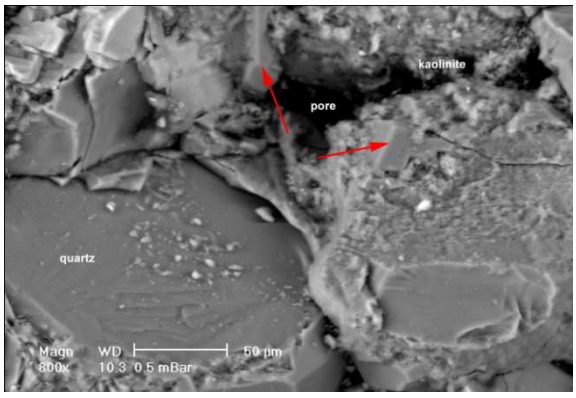

Figure 3: SEM image of Donnybrook sandstone

The micro-CT images of the Donnybrook sample do not have sufficient contrast in X-ray density between different minerals, and hence do not allow reliable discrimination between these minerals. Thus the bulk and shear moduli of the solid phase are calculated by means of the effective medium theory. Self-consistent approximation (SCA) (Berryman, 1980) is used to obtain effective moduli. This approximation was specifically designed to provide estimates that are symmetric with respect to all constituents (that is, it does not treat any constituent as a host or inclusion). Bulk and shear moduli are chosen as 39 and 33 GPa for quartz (Han et al., 1986), 76 and 26 GPa for plagioclase feldspar (Woeber et al., 1963) and 12 and 6 GPa for kaolinite (Vanorio et al., 2003), respectively. Assuming (from SEM images, Figure 3) that the aspect ratio of the grains is about 1, we obtain effective bulk and shear moduli of the solid phase of 37 GPa and 27 GPa, respectively.

For numerical simulation of elastic moduli of the sandstone sample, we use finite element method that has been utilized in a number of works for elastic (and poroelastic) simulations. The simulations are performed by means of ABAQUS FEA software. To simulate P-wave modulus *M*, a normal displacement is applied to one of the faces, for instance, to the top of the sample, while on all other faces the normal displacements are set to zero. The modulus is then calculated as $M = \langle \sigma_x \rangle / \langle \varepsilon_x \rangle$, where the angle brackets mean averaging over all the elements. Then, to simulate shear modulus *G*, a shear displacement is applied to the top face while the opposite face is kept fixed. The bulk moduli is then calculated as $K = M - 4/3\mu$. In this study we assume the sample is isotropic and, thus, the choice of faces of loading and directions of displacement is not important.

The method described above is applied to each of the eight subvolumes of the original cube. Porosities of the subvolumes calculated from the segmented microtomograms vary from 12% to 22%. This porosity variability allows estimation of the dependency of elastic moduli on porosity. The results of the simulations are shown in Figure 4 in comparison with the estimations of SCA method (Berryman, 1980) for inclusions of different regular shapes, namely, spheres (aspect ratio 1) and oblate spheroids with aspect ratios from 0.01 to 0.5. The simulated moduli are in a good agreement with those obtained by SCA for the regular shape inclusions with aspect ratios from 0.2 to 1.

Comparison with experimental data

The results of numerical simulations are shown in Figure 5 in comparison with experimental data obtained for a Donnybrook sandstone sample at effective stresses of 0-70 MPa at ultrasonic frequencies. Note that the simulated moduli are shown for the part with porosity of 15%, which is the porosity of the sample employed for ultrasonic measurements. The experimental data are shown by solid circles with error bars. The results of numerical simulations obtained from CT images at ambient pressure are shown by horizontal lines. Linear trends that characterize variations of measured elastic moduli at high pressures of 50-70 MPa are shown by dashed lines.

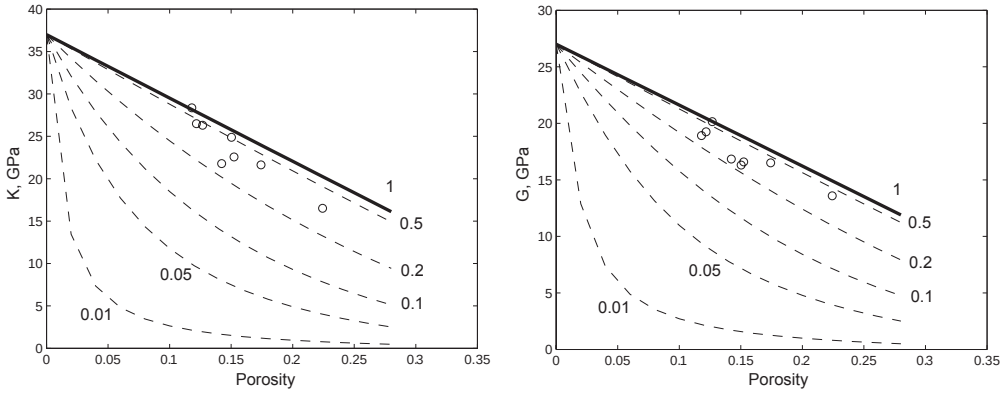

Figure 4: Bulk and shear moduli simulated for all parts (circles) in comparison with SCA method predictions for pores of different shapes from spheres (solid line) to oblate spheroids with aspect ratios (0.01-0.5) (dashed lines).

One can see that the numerically simulated moduli strongly overestimate the measured ones at low effective stresses of 0-50 MPa, then at 50 MPa, the simulated and experimental moduli are in a good agreement and, finally, at effective stresses higher than 50 MPa the measured moduli exceed the simulated ones. To explain these differences, three distinct effective stress ranges should be analyzed separately. We assume that at low effective stresses, the elastic moduli are strongly affected by compliant porosity represented by grain contacts and microcracks (e.g., Shapiro, 2003: Pervukhina et al., 2010). Such microcracks reduce elastic moduli dramatically at lower stresses. We note that compliant porosity is unresolvable by micro-CT and thus is not taken into account in our numerical simulations. Therefore, for the same stress level, the numerical simulations overestimate elastic properties. As compliant porosity decreases exponentially with an effective stress increase (Pervukhina et al., 2010; Becker et al., 2007), the discrepancy between measured and simulated moduli diminishes at higher effective stresses of 30-40 MPa and, finally, measured moduli reach numerically simulated ones at the stresses of ~50 MPa, at which compliant pores are closed. At still higher stresses of 50-70 MPa, the linear trend of the experimentally measured elastic moduli variations with stress indicates a decrease of stiff porosity as shown by (Mavko and Jizba, 1991). The numerical simulations do not take into account this reduction of porosity (as the microtomograms are obtained at zero stress) and, thus, underestimate the experimentally measures elastic moduli.

Conclusions

A new rock physics workflow including 3D imaging, processing and simulations of physical experiments fulfilled using widely available software, namely, AVIZO (Visualization Sciences Group) and ABAQUS FEA (SIMULIA) is developed. The advantage of general-purpose software is two-fold: (1) it allows extension to more complex rheological models and (2) it employs diverse tools (such as adaptive grids) developed for diverse applications. Elastic moduli of a Donnybrook sandstone are numerically simulated using microtomograms. The simulated and measured elastic moduli are in a good agreement at the effective stress of about 50 MPa.

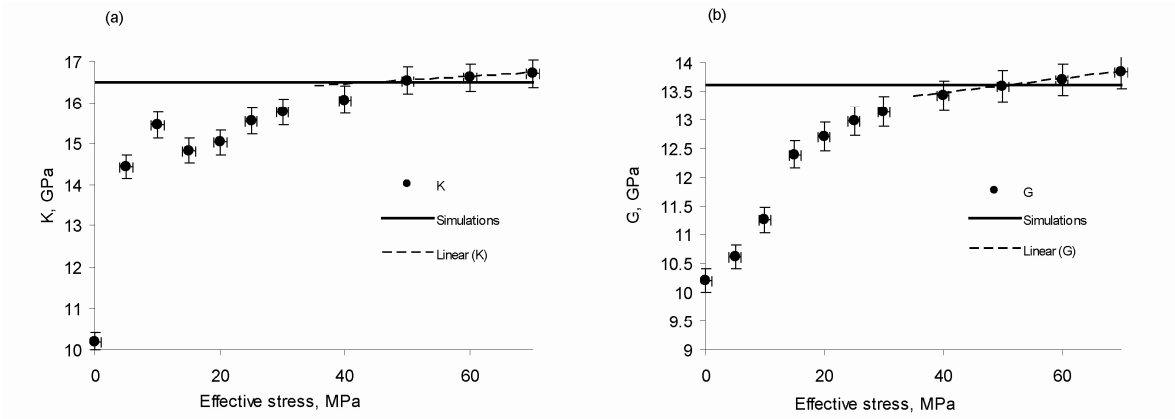

Figure 5: Comparison of simulated bulk (a) and shear (b) modili (solid line) with experimental data (circles) for Donnybrook sandstone measured for effective stresses 0-70 GPa. Linear trend observable at effective stresses of 50-70 MPa is marked with a dashed line

Acknowledgements

We would like to acknowledge Claudio Delle Piane for useful discussion and iVEC for ability to use their supercomputer facilities, AVIZO software. We thank Andrew Squelch for priceless advice and technical support.

References

Arns, C.H., Knackstedt, M.A., Pinczewski, W.V., Garboczi, E.J., 2002, Computation of linear elastic properties from microtomographic images: Methodology and agreement between theory and experiment, Geophysics, 67(5), 1396-1405.

Becker, K., S. A. Shapiro, S. Stanchits, G. Dresen, and S. Vinciguerra (2007), Stress induced elastic anisotropy of the Etnean basalt: Theoretical and laboratory examination, Geophys Res Lett, 34(11), L11307

Berryman, J. G. 1980. Long-wavelength propagation in composite elastic media II. Ellipsoidal inclusions. *J. Acoust. Soc. Am.*, 68 (6), 1820-1831.

Dvorkin J., 2009, Accuracy and Relevance of Digital Rock Results: Successes and Failures, Ingrain Digital Rock Physics Lab, 1-22.

Garbozci, E.J., 1998. Finite element and finite difference programs for computing the linear electrical and elastic properties of digital images of random materials. National Institute of Standards and Technology Internal report.

Han, D.-H., A. Nur, and D. Morgan, 1986, Effects of porosity and clay content on wave velocities in sandstones, Geophysics, 51, 2093-2107.

Mavko, G., and D. Jizba (1991), Estimating Grain-Scale Fluid Effects on Velocity Dispersion in Rocks, Geophysics, 56(12), 1940-1949.

Pervukhina, M., B. Gurevich, D. N. Dewhurst, and A. F. Siggins, 2010, Experimental verification of the physical nature of velocity-stress relationship for isotropic porous rocks, Geophysical Journal International.

Roberts, A. P., and Garboczi, E. J., 2000, Elastic properties of model porous ceramics: J. Amer. Ceramic Soc., 83, 3041–3048.

Saenger, E., Ciz, R., Kruger, O., Schmalholz, S., Gurevich, B, Shapiro, S., 2007, Finite-difference modeling of wave propagation on microscale: A snapshot of the work in progress. Geophysics 72 (5), 1293-1300,

Sayers and Kachanov,1995 Microcrack-induced elastic wave anisotropy of brittle rock, J.G. Res., 100, 4149-4156

Shapiro, S. A. 2003, Elastic piezosensitivity of porous and fractured rocks, Geophysics, 68(2), 482-486.

Vanorio, T., M. Prasad, and A. Nur, 2003, Elastic properties of dry clay mineral aggregates, suspensions and sandstones, Geophysical Journal International, 155, 319-326.

Woeber, A. F., S. Katz, and T. J. Ahrens, 1963, Elasticity of selected rock and minerals, Geophysics, 28, 658-663.